# One-Step Method for the Fabrication of Pure and Metal-decorated Densified CNT Films for Effective Electromagnetic Interference Shielding

*Fan Yang*[a], *Shengcun Ma*[a], *Chia Miang Khor*[a], *Yiming Su*[a], *Zahra Barani*[b], *Zhenpeng Xu*[a], *Arthur Boyko*[c], *Arpita Iddya*[a], *Naama Segev-Mark*[c], *Xiaoyu (Rayne) Zheng*[a, f], *Fariborz Kargar*[b], *Alexander A. Balandin*[b], *Guy Ramon*[c], *Igor De Rosa* [d,e], *Eric Hoek*[a, f, h, i] *and David Jassby*[a, f, h, *]

[a]Department of Civil & Environmental Engineering, University of California, Los Angeles (UCLA), Los Angeles, 90095, USA

[b]Department of Electrical and Computer Engineering, University of California, Riverside (UCR), Riverside, 92521, USA

[c]Department of Civil & Environmental Engineering, Technion – Israel Institute of Technology, Haifa, 32000, Israel

[d]Institute for Carbon Management, University of California, Los Angeles (UCLA), Los Angeles, 90095, USA

[e]Materials Science and Engineering, University of California, Los Angeles (UCLA), Los Angeles, 90095, USA

[f]California NanoSystem Institute, UCLA, Los Angeles, 90095, USA

[h]Institute of the Environment & Sustainability, UCLA, Los Angeles, 90095, USA

[i]Energy Storage & Distributed Resources Division, Lawrence Berkeley National Lab, Berkeley, 94720, USA

**Corresponding Author**

*__David Jassby__. Tel: (310) 825-1346. E-mail: jassby@ucla.edu

ABSTRACT

Light-weight, thin, and robust electromagnetic shielding materials with high electrical conductivity are needed for advanced modern electronics and telecommunication technologies to protect circuits from electromagnetic interference. Carbon nanotubes (CNT) are ideal candidates for electromagnetic shielding materials due to their excellent mechanical strength, high electrical conductivity, and light weight. However, the relatively poor electrical conductivity of CNT films, a result of the many points of contact resistance between neighboring CNTs, is an obstacle towards their utilization as a shielding material. Here, we propose a facile CNT film fabrication method that enhances the conductivity of CNT films by collapsing the separation between neighboring CNTs (i.e., densifying the material) in the CNT network. The dense CNT films resulting from this facile method exhibit high electrical conductivity (~$10^6$ S m-1), and achieve excellent shielding of 99.999992% (71 dB) at frequencies between 8.2 GHz and 12.4 GHz with a thickness of 14.3 $\mu$m. The remarkable absolute shielding effectiveness (3.50 x $10^5$ dB $cm^{-2}$ $g^{-1}$) is due to the material's low density (i.e., ~1.0 g/$cm^3$), thinness (i.e., 1.3 to 14.3 $\mu$m), and metal-like conductivity. Also, the produced CNT sheet is an ideal substrate for gold decoration that can dramatically enhance the EMI shielding performance further (EMI SE increased from 43.90 dB in the loose film to 56.67 dB in the dense film, which further increased to 66.12 dB when the dense CNT film was coated with a thin gold layer). The outstanding properties of gold-decorated dense CNT films make them strong candidates to meet the electromagnetic shielding needs of modern cutting-edge, lightweight, and compact electronic devices.

Keywords: carbon nanotube film, electrical conductivity enhancement, electromagnetic interference shielding

## 1. INTRODUCTION

There is a critical need to attenuate electromagnetic interference (EMI) in electronic components and devices[1-3]. EMI is produced by electromagnetic fields that are generated by devices that use or transmit electricity (e.g., phones, electric vehicles, and power strips)[4]. Therefore, materials that act as a shield by reflecting and/or absorbing electromagnetic radiation producing high EMI shielding effectiveness (EMI SE) are highly desired. Development of high EMI SE materials with easy processability, light weight, minimum thickness, and has become important due to the EMI shielding requirements of modern cutting-edge fields like aerospace materials, high-speed telecommunication and ultra-microelectronics[1, 5].

Conventional metallic shielding materials, such as copper and silver, can achieve excellent EMI SE due to their intrinsically high electrical conductivity. However, their high density (e.g., 8.94 g $cm^{-3}$ for Cu and 10.49 g $cm^{-3}$ for Ag) and susceptibility to corrosion limits their applications as EMI shields, especially for advanced electronics[4, 6]. Lightweight polymer/conductive filler composites, owing to the high conductivity of the flexible fillers, such as metal wires[7-9], graphene/graphite[10-12], quasi-1D filters[13], and carbon nanotubes (CNT) have also been proposed for EMI shielding[14]. However, most polymers are insulators, and lead to poor connectivity between adjacent conductive fillers, which reduces the conductivity of the polymer composite, a critical aspect of EMI shields[14-16]. Additionally, the low durability of polymeric materials and their poor anti-bacterial properties further reduce their adoption as EMI shields in electronics[9]. In addition to polymer/filler composites, nanostructured assemblies of conductive materials like percolating networks of CNTs, reduced graphene oxide (rGO), and 2D metal carbonitrides (MXene) have also been explored as EMI shielding materials[1, 4, 17, 18].

Individual CNTs are known to be nearly perfect molecular wires with outstanding structural, electrical, and thermal abilities[19]. The electrical conductivity of an individual CNT has been determined to be as high as $2 \times 10^7$ S $m^{-1}$[20], with a tensile strength of up to 150 GPa[21, 22]. However, poor nanoscale contacts and high junction resistance between neighboring CNTs in a percolating network undermine the electrical and mechanical properties, as well as the EMI shielding performance of CNT films. As a result, typical CNT films exhibit ~ 1% of their potential electrical conductivity and tensile strength compared to an individual CNT[23-25]. This poor electrical conductivity of CNT films has limited their use as a shielding material. Chlorosulfonic acid (CSA) is known as an excellent solvent and functionalization agent for the dispersal and sulfonation of CNTs[26, 27]. Taking advantage of these properties, researchers have been using CSA to densify CNT network using a rather complex sequence of steps: 1) the CNT network is thermally annealed (to remove amorphous carbon impurities), 2) the CNT network is soaked in sulfuric acid to further remove residual metallic catalysts, 3) the CNT network is then soaked in CSA, and allowed to dry, which produces the densified film[28]. Although these membranes display strong EMI shielding properties, the cost (i.e. the energy required for thermal annealing, additional sulfuric acid consumption), and complexity of the treatment processes (i.e. the need to first make a loose CNT network and multiple physical and chemical processing steps) limit its potential for larger scale applications. In this study, we use a facile one-step fabrication method based on the evaporation of CNT-acid suspensions to produce a metal-like conductive CNT film for EMI shielding. Furthermore, the densified CNT network serves as an excellent substrate for the facile decoration with gold particles (or other metals), leading to further enhancement of the film's conductivity and electromagnetic interference (EMI) shielding properties. The difference in Fermi levels between Au (III) and CNT facilitates the rapid and simultaneous reduction of Au (III)

to Au(0) on the densified CNT network, contributing to these improved properties[29].While previous studies have demonstrated a multi-step process towards the same goals, here we demonstrate a highly simplified and scalable fabrication method that results in a material whose EMI shielding exceed materials fabricated using previously reported methods[26, 28]. Specifically, CNTs suspended in CSA are spread over a substrate and the CSA is evaporated, which results in a densified, highly conductive thin-film material with uniform properties and excellent EMI shielding properties (Fig.1). In contrast, previous methods used to produce densified CNT films relied on multi-step processes. Other methods include the pre-alignment of CNTs using a rotating drum followed by the spraying and evaporation of ethanol; the produced film had a strength of 9.6 GPa with a thickness of 120 nm after further physical compression, but the authors did not describe the electrical properties of the material[21] Other methods based on CNT arrays (i.e. CNT forests grown on the substrate) by domino-pushing (i.e. physically pushing down a CNT forest followed by compression), shear pressing, and dry drawing have also been used to produce CNT films with good mechanical strength and reasonable electrical properties[30-32]. Aligned CNT films fabricated via domino pushing had an electrical conductivity of $2.0 \times 10^4$ S $m^{-1}$ compared to that of $1.5 \times 10^4$ S $m^{-1}$ for random oriented samples[30]; CNT films with a thickness of 40 um produced from shear pressing exhibited a conductivity of $1.18 \times 10^4$ S $m^{-1}$ parallel to the CNT axis and 0.42 $\times 10^4$ S $m^{-1}$ perpendicular to the CNT axis, and a tensile strength of 402 MPa[31]; thin densified CNT sheets with a thickness of 50 nm made by dry drawing showed a conductivity of $2.86\times 10^4$ S $m^{-1}$ along the aligned CNT direction, and a tensile strength ranging between 87.5 MPa and 232.5 MPa, depending on the degree of alignment[32]. In general, all previous fabrication methods either involved a multi-step process or resulted in films with relatively poor electrical properties that would minimize their usefulness as EMI shields. The one-step CNT densification method in this

study has a greater potential for scale-up, is more sustainable in terms of energy and chemical consumption, and produces an ultra-conductive, strong, and highly EMI shielding material.

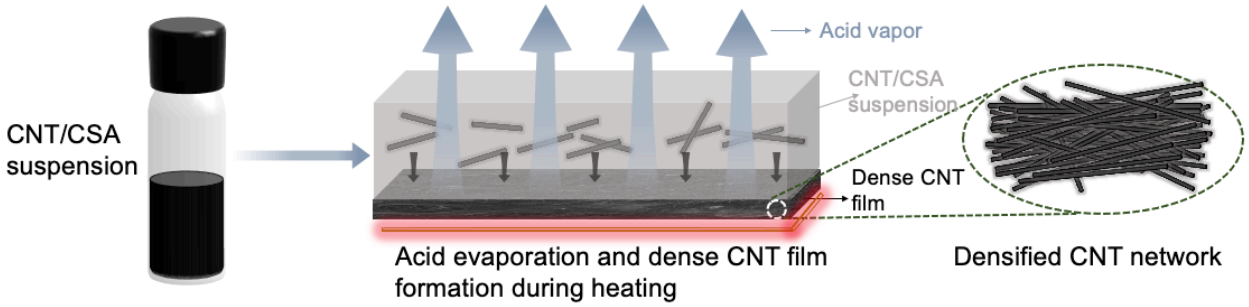


**Fig. 1.** schematic diagram of dense CNT film fabrication process.

## 2. EXPERIMENTAL SECTION

**2.1. Materials.** Carboxyl group functionalized single-walled CNT (SWNT-COOH) with a diameter of 1-4 nm was purchased from Cheap Tubes Inc. (USA). Concentrated sulfuric acid ($H_2SO_4$), Sodium hydroxide (NaOH, 10N), sodium dodecylbenzene sulfonate (SDS), and Dimethylformamide (DMF) were purchased from Fisher-Scientific. CSA and lime soda were purchased from Sigma-Aldrich. Polysulfone UF membranes (PS35, molecular weight cut-off of 20 kDa) were kindly provided by Solecta Membranes (USA). Tetrachloroauric(III) acid trihydrate ($HAuCl_4 \cdot 3H_2O$, 99.9%) was purchased from Sigma Aldrich.

**2.2. Fabrication of dense CNT film.** Dense CNT films with various thicknesses were prepared via a thermal-induced evaporation process by varying the amount of CNTs in a CNT/CSA suspension. A 1 g $L^{-1}$ CNT/CSA solution was prepared by dispersing 10 mg of CNTs into 10 ml CSA in a glass vial. The CNTs/CSA dispersion was stirred mildly for 3 hours on a stir plate at room temperature, prior to being poured onto a glass petri dish on a heating plate. The glass petri dish with CNT/CSA solution was then covered with a funnel, which acted as a vapor guide. The emanating vapors were directed into a gas washing bottle, containing lime soda, via the funnel

using a vacuum. At the beginning of the thermal-assisted evaporation process, the temperature of the heating plate was controlled at 100 ºC, which is below the boiling point of CSA (around 150 ºC). As the glass petri dish heated up, the acidic vapor emanating from the CNT/CSA suspension was absorbed and neutralized by lime soda in the gas washing bottle. The subsequent evaporation of CSA led to the formation of the CNT film; the temperature was then switched to 140 ºC for 0.5 hours to remove any residual acid present in the CNT film. Finally, the prepared CNT film was washed thoroughly by placing the petri dish with the dense CNT film into a water bath.

**2.3. Preparation of CNTs film by pressure-assisted filtration.** In order to fabricate CNT film on polymeric support, 1g CNT was suspended in 1L of deionized water together with 10 grams of SDS as surfactant. This CNT suspension was then sonicated with a probe ultrasonicator (120C, Branson, USA) in an ice water bath for 30 mins (1s on, 1s off) followed by centrifugation for 15 min at 14,000 rpm three times to remove unsuspended particulates. 45 ml of this CNT stock solution was then pressure-deposited on a porous PS35 UF membrane at 40 psi. The prepared CNT-coated UF membrane was washed thoroughly with 1 L of deionized water to flush out the nonattached surfactant and dried at 80 ºC for 30 mins.

**2.4. Fabrication of free-standing filter-deposited porous CNT film.** To obtain the free-standing porous CNT film from the PS35 support membrane, the CNT coated- UF membrane was first rinsed in a warm DMF bath until the PS35 support separated from the CNT film layer. The CNT film was then thoroughly washed in another DMF bath, followed by soaking in a water bath. Finally, the produced free-standing CNT film was dried at 80 ºC for 30 min prior to characterization.

**2.5. Acid/alkali treatment of dense CNT film.** 1mol $L^{-1}$ $H_2SO_4$ and 1mol $L^{-1}$ NaOH solution were prepared out of concentrated $H_2SO_4$ and 10 N NaOH, respectively. The dense CNT films

were rinsed in the prepared 1mol $L^{-1}$ acid bath or 1 mol $L^{-1}$ alkali solution bath for one hour. The treated dense CNT films were then thoroughly washed with DI water followed by drying at 80 ºC for 30 min.

**2.6. Fabrication of dense CNT/Gold film.** A 20 mM gold ion solution was prepared by adding 0.157 g Tetrachloroauric (III) acid trihydrate to 20 ml deionized water followed by sonication for 2 min. The dense CNT film was soaked in the gold ion solution in a glass jar for 20 min to complete the reduction of $Au^{3+}$ to $Au^0$: $AuCl_4^- + 3e^- \leftrightarrow Au + 4Cl^-$. The reduction of $Au^{3+}$ to $Au^0$ is enabled by the difference in the Fermi levels of the CNTs and Au(III) (+0.5 V compared to the standard hydrogen electrode (SHE) for CNTs, vs. +1.002V vs. SHE for $AuCl_4$) [29] [33]. Subsequently, the SWCNT film was taken out from the solution and washed thoroughly with deionized water. The densified gold-coated SWCNT (CNT/gold) film was then dried in an oven at 80 °C overnight and smoothed using mechanical rolling, where the CNT/gold membrane was first wet with ethanol and then rolled several times between two rollers running in opposite directions with different gaps (from 10 um to 5 um).

**2.7. Materials Characterization.** The electrical conductivity of films was calculated from their sheet resistance using a 4-point-probe conductivity meter (MCP-T610, Mitsubishi Chemical Analytech Co., Japan). The film morphology and the cross-sectional structure were studied using a scanning electron microscope (SEM) (Zeiss SUPRA 40-VP) and Nova 600 SEM/FIB system, respectively. Contact angle measurements were performed using a contact angle goniometer (250-U1, rame-hart instrument co., USA). The chemical composition of the CNT film's surface was determined using X-ray photon spectroscopy (XPS) (Kratos Axis Ultra DLD spectrometer equipped with a monochromatic Al Kα X-ray source). XPS data was processed using CasaXPS software (version 2.3.18). The tensile strength of CNT films was tested using a ~5mm x 25mm

strip. Unidirectional tensile tests were performed using Instron 5944 with a 500N load cell to evaluate the corresponding stress-strain curves (Reference standard: ASTM – D882). A strain rate of $10^{-3}$ $s^{-1}$ was applied on each sample until fracture. The effective stiffness was calculated by testing linearity via the least-squares regression technique. X-ray diffraction (XRD) measurements were performed on a Panalytical X'Pert Pro X-ray powder diffractometer (Malvern Panalytical, Netherlands) using Cu Kα1 radiation under double axis diffraction condition. The step size of the 2θ–ω scans was 0.02° and the scan speed time was 0.1 °/s.

**2.8. Electromagnetic Interference Shielding Measurement.** Evaluation of EMI shielding performance in X-band frequency range of CNT films was carried out using a vector network analyzer (VNA) (N5247A, Agilent, USA) via the coaxial method. The samples were cut into a 25 mm x 12 mm strip to fit the waveguide window (22.86mm x 10.16 mm). Before data collection, two working ports of the VNA were calibrated using the standard SSLT method. For each experiment, scattering parameters (S11, S22, S12, and S21) were recorded for EMI SE calculation.

**2.9. Theoretical Calculations of EMI shielding effectiveness.** EMI SE (dB) displays the ability of a material to attenuate the incident EM waves. The total EMI SE ($SE_T$) is composed of three components: reflection shielding ($SE_R$), absorption shielding ($SE_A$), and multiple reflections shielding ($SE_M$). Generally, the $SE_M$ can be neglected when the $SE_T$ is larger than 15 dB[3].

$$SE_T = SE_R + SE_A + SE_M \tag{2}$$

In order to calculate the $SE_T$, $SE_R$, and $SE_A$, reflectivity (R) and transmission (T) values need to be obtained from their coefficients (r and t, respectively) in terms of scattering parameters.

$$R = |r|^2 = |S_{11}|^2 \tag{3}$$

$$T = |t|^2 = |S_{12}|^2 \tag{4}$$

202 $SE_T$, $SE_R$, and $SE_A$ can further be calculated as follows

203 $$SE_T = 10\log(\frac{1}{T}) = 10\log(\frac{1}{|t|^2}) \quad (5)$$

204 $$SE_R = 10\log(\frac{1}{1-R}) = 10\log(\frac{1}{1-|r|^2}) \quad (6)$$

205 $$SE_A = 10\log(\frac{1-R}{T}) = 10\log(\frac{1-|r|^2}{|t|^2}) \quad (7)$$

206 Calculation of Absolute Shielding Effectiveness: prior to calculating the absolute shielding
207 effectiveness, specific shielding effectiveness (SSE) is required. SSE is defined by normalizing
208 shielding effectiveness with the density (SE/density, dB $cm^3$ $g^{-1}$). Absolute shielding effectiveness
209 is then calculated by dividing SSE with the thickness (SSE/t), taking both density and thickness of
210 materials into account: $SSE/t = SE/(density \cdot t)$ (dB $cm^2$ $g^{-1}$).

211 3. RESULTS AND DISCUSSION

212 Reducing the contact resistance by decreasing the distance between individual CNTs can
213 significantly improve the conductive performance of CNT networks since the intrinsic resistance
214 of CNTs is negligible compared to contact resistance between neighboring CNTs in a network
215 (i.e., resistance caused by electron tunneling) [34, 35]. The facile fabrication process of the metal-
216 like CNT film is illustrated in Fig.1. CSA, an excellent solvent for CNTs, was used to disperse
217 single-walled CNTs (Fig. 2a). Low concentration CNT dispersions in CSA exhibit an isotropic
218 phase with random orientation[27] . However, as the concentration increases, the CNTs transition
219 into a liquid-crystalline (LC) phase, where the CNTs become densely packed and aligned due to
220 excluded volume effects[26]. Between these extreme conditions (i.e., medium concentrations), a
221 biphasic phase of CNTs is formed [26]. CSA, a true solvent of CNTs, exhibits the highest

222 solubility of individual CNTs, where CNTs are well dispersed (i.e. in an isotropic phase) when
223 their concentrations are below 0.61 vol%[26]. The highly polar CSA is capable of polarizing
224 individual CNTs, enhancing the attractive forces between adjacent polarized CNTs[28]. As a
225 result, when the CSA evaporates, the CNT network collapses and forms a dense film (Fig.2b). The
226 dense CNT film has a metallic, reflective appearance, reflecting light off of the surface (Fig. 2b
227 and Fig. 2c). The dense CNT film shows enhanced electrical conductivity ($0.78 \times 10^6 \pm 4.85 \times$
228 $10^4$ S $m^{-1}$), which is two orders of magnitude higher than traditional CNT-based films (i.e., ~$10^4$ S
229 $m^{-1}$) [36], and comparable to conductive metals (e.g., ~$1 \times 10^6$ S $m^{-1}$ for stainless steel) [37]. A
230 pressure-deposited porous CNT film was used as a comparison with the dense CNT film in terms
231 of conductivity and morphology. The surface of dense CNT films was imaged using scanning
232 electron microscopy (SEM), and shows individual CNT and CNT bundles tightly packed with no
233 observable gaps between them (Fig. 2d and 2e). Cross-sectional images of the dense CNT film
234 show the dense structure of CNT network and the close packing of CNTs (Fig. 2f). In contrast,
235 porous CNT films fabricated by pressure-depositing a CNT/surfactant suspension show a very
236 loose CNT network with large pores between neighboring CNTs (Figs. 2g – 2i). The porous
237 structure of the film was also observable in a cross-sectional image of the material (Fig. 2i). When
238 the dense CNT membrane was coated with gold and mechanically rolled, a shiny metallic golden
239 is obtained (Fig. 2j). Initially, the CNTs, acting as electron donors, reduce Au (III) ions in the
240 solution to metal Au, resulting in the formation of gold clusters on the surface of the CNT film and
241 within the porous film. As these gold clusters grow larger and form a continuous layer, they
242 interlock with the CNT network at the interface. The interlocking mechanism involves the
243 interplay of van der Waals forces, which contribute to the interfacial interactions and subsequently
244 influence the mechanical properties of the film. After the mechanical compaction process, the

separation distance between the two layers at the interface and between the gold particles decreases. This closer proximity enhances the van der Waals forces, both between the layers and among the gold particles. These strengthened van der Waals forces contribute to improved interfacial adhesion and cohesion. SEM image analysis reveals a crystal-like gold layer on the surface of the densified CNT network. (Figs. 2k-l).

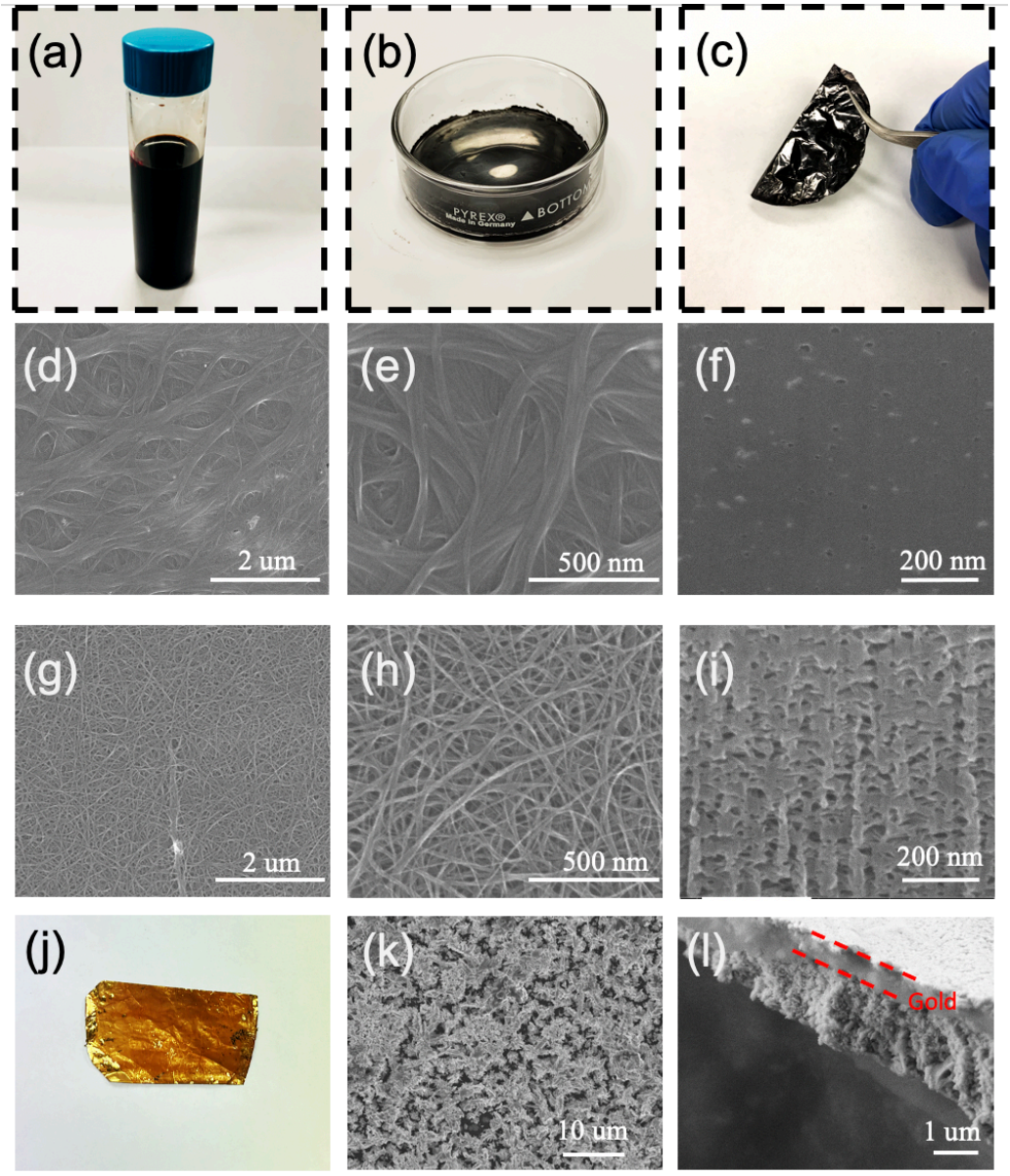


**Fig. 2.** (a) CNT/ CSA suspension in glass vial. (b), (c) Light - reflecting dense CNT films with patches of light reflecting off: (b) Photo of dense CNT film in glass petri dish after evaporation of

CSA, (c) photo of free-standing dense CNT film peeled from petri dish. (d), (e) Low-magnification (d) and high-magnification (e) SEM images of surface morphology of dense CNT film. (f) SEM image of dense CNT film from cross-sectional view. (g), (h) Low-magnification (g) and high-magnification (h) SEM images of surface morphology of a pressure-deposited porous CNT film. (i) SEM image of a pressure-deposited porous CNT film from cross-sectional view. (j) photo of dense CNT coated with gold. (k) SEM image of the surface of dense CNT film coated with gold. (l) Cross-sectional view of dense CNT film with gold coating.

The electrical conductivity of the dense CNT film was a function of its thickness, with the highest conductivity ($0.78 \times 10^6 \pm 4.85 \times 10^4$ S m$^{-1}$) measured at a film thickness of 2.8 $\mu$m (Fig. 3a); this value is ~ 2.7 times higher than that of a non-densified, porous CNT film ($2.92 \times 10^5 \pm 1.11 \times 10^4$ S m$^{-1}$) (Fig. 3a, and Table S1). The conductivity of the CNT/gold membrane with a total thickness of 3.3 $\mu$m increased to $2.31 \times 10^6 \pm 3.60 \times 10^4$ S m$^{-1}$, a nearly 8-fold increase compared to the non-densified CNT film. At a low thickness of 1.3 $\mu$m, a small amount of CNTs within a certain volume may not form a tightly packed film. Consequently, the uneven distribution of CNTs can result in regions with fewer CNTs compared to other regions. These low-density regions, characterized by large gaps between CNT individuals/bundles, can introduce additional resistance when the thickness is small[38]. However, as the thickness increases, the number of these low density regions declines and the conductivity of the CNT network stops increasing with thickness, stabilizing at $0.78 \times 10^6$ S m$^{-1}$ at 2.8 $\mu$m. XRD spectrum analysis demonstrates the successful growth of Au on the dense CNT network (Fig. 3b): the diffraction peaks at 38.4°, 44.6°, 64.7°, 77.71°, and 81.85° can be assigned to (111), (200), (220), (311), and (222) crystalline diffraction planes of Au. Au diffraction peaks correspond to the typical face-centered cubic crystal structure and does not indicate the presence of any intermetallic gold compounds. Furthermore,

the Au (111) peak exhibits strong intensity compared to those of Au (200), Au (220), and Au (311) planes. The relative intensity of Au (200)/Au (111) is 0.27, lower than the bulk gold value (0.52 from JCPDS #04–0784), indicating the synthesized Au film were highly (111) oriented [39].

The high conductivity of the dense CNT film is a result of the dense CNT network that reduced the resistance to electron transport between neighboring CNTs, which is highly sensitive to the separation distance between conducting strands in a network[30, 40, 41]. In contrast, for the pressure-deposited CNT film, the large gaps between neighboring CNTs (Fig. 2h) increased the electron hopping distance and reduced the membrane conductivity.

The mechanical strength of the CNT films, evaluated from the tensile stress-strain curves, showed that the dense CNT films had enhanced mechanical properties (Fig. 3c). Specifically, the ultimate strength of the dense CNT film, calculated by dividing the applied force by the cross-sectional area of the film, was 161.5 ± 25.6 MPa at 2.16 ± 0.52 % deformation. In contrast, the ultimate strength and maximum deformation of the porous CNT film were 106.6 ± 2.0 MPa and 2.54 ± 0.25 %, respectively. The ultimate strength of the dense CNT film (161.5 MPa) is 1.52 times higher than that of a porous CNT film because the CSA-induced densification shortens the separation distance. As a result, the attractive van der Waals force between adjacent CNTs is enhanced[42], and the dense CNT network shows stronger mechanical properties. Based on the stress and strain values at failure, the Young's modulus of dense and porous films was calculated to be 10.85 ± 0.67 GPa and 6.99 ± 0.25 GPa, respectively (details in Table S2). The ultimate strength of a dense CNT film was found to be higher than that of aluminum (~110 MPa). However, its stiffness is much lower than that of aluminum (~69 GPa), suggesting that this light-weight film has superior mechanical strength and excellent flexibility. Additionally, the film can be folded and twisted without any damage, as shown in Supporting Information.

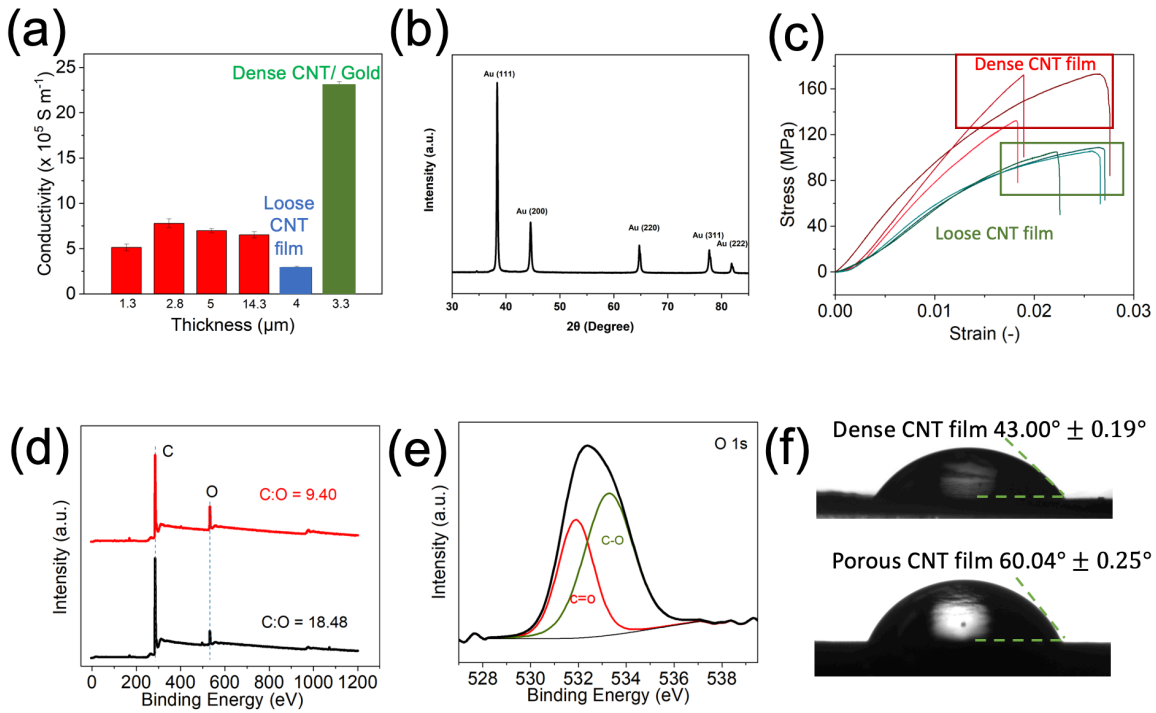


299

300 **Fig. 3.** (a) Changes in electrical conductivity of dense CNT films as a function of thickness (red),
301 compared with porous CNT films (blue). (b) XRD spectrum of dense CNT/Au film. (c) Stress –
302 strain curve of dense CNT films (red) and porous CNT films (blue) with a thickness of 2.8 $\mu$m. (d)
303 XPS survey spectra of a dense CNT film (red line) and porous CNT film (black line). (e) High
304 resolution spectra of O 1s of a dense CNT film. (f) Water contact angle measurements of a dense
305 and porous CNT film.

306 X-ray photoelectron spectroscopy (XPS) survey spectra of a dense and porous CNT film
307 exhibited sharp peaks associated with C and O, originating from the carbonous CNT backbone and
308 surface functional groups (Fig. 3d). After CSA evaporation, the C/O ratio of dense CNT film was
309 9.40, lower than the 18.48 ratio found on porous films, which can be attributed to the partial
310 oxidation of CNTs by the strong acid CSA. A high-resolution XPS scan of O1s shows that the
311 ratio of C = O/C – O for the dense CNT film is 0.61, while the C = O/ C – O ratio is only 0.35 for

312 a porous CNT film (Fig. 3e and Fig. S2). The larger number of C = O groups in the dense CNT
313 film further supports the observation that the immersion of the CNTs in CSA led to the oxidation
314 of surface carbon groups. The oxidation of dense CNT film is also evident through the contact
315 angle measurements of the porous and dense films (Fig. 3f). The contact angle of a porous film
316 (60.0 ± 0.3°) was determined to be higher than that of a dense CNT film (43.0 ± 0.2°). The lower
317 contact angle of the dense CNT film suggests the presence of more polar surface groups, which
318 can be attributed to the oxidation of carbon groups (e.g., carboxyl and carbonyl groups). It is indeed
319 worth noting that the conductivities of dense CNT films exhibit an increase, even when the
320 individual CNTs within them are oxidized (as shown in Fig. 3a). Generally, CNTs without any
321 defects tend to possess higher conductivity compared to CNTs with functional groups [43].
322 However, in the case of the dense CNT film, the overall conductivity increase can be attributed to
323 the decrease in contact resistance, which arises from the densification of the CNT network, which
324 more than offsets the decrease in conductivity resulting from the CNT oxidation.
325 Due to their dense structure, intrinsically high electrical conductivity and multiple functional
326 groups, dense CNT films show exceptionally high EMI SE values. Fig. 4a shows the total EMI
327 shielding effectiveness ($SE_T$) of a dense CNT film with different thicknesses (1.3 $\mu$m, 2.8 $\mu$m,
328 5$\mu$m, and 14.3 $\mu$m) over the X-band frequency range (8.2 GHz – 12.4 GHz). It is noted that $SE_T$
329 increased with an increase in film thickness. Yet, even the thinnest dense film (1.3 $\mu$m) has a $SE_T$
330 of 50.5 ± 1.3 dB, and demonstrates ~99.999% blockage of incident EM waves, which is higher
331 than the commercial EMI shielding requirement (40 dB) [44]. The $SE_T$ reaches as high as 71 ± 2.1
332 dB with a film thickness of 14.3 $\mu$m, suggesting that 99.999992% of EM waves are attenuated by
333 the dense CNT film. Compared with the loose CNT film, the dense CNT film's $SE_T$ was 12.77 dB
334 higher at same thickness (i.e. 2.8 $\mu$m) (Fig. 4b). The dense CNT/Au films shows a further

enhancement of EMI SE compared to the uncoated dense film; the EMI SE over the whole X band was lifted by 22.22 dB after the Au coating, reaching a value of 66.12 dB for a dense CNT/Au film (the total thickness of new CNT/gold film is 3.3 $\mu$m) (Fig. 4b). To deconvolute the $SE_T$ value in terms of the EMI shield's properties, we used Simon's formula[45]:

$$SE_T = 50 + 10\log(\sigma / f) + 1.7t(\sigma f)^{0.5} \quad (1)$$

where $\sigma$, $f$, and $t$ represent electrical conductivity (S cm$^{-1}$), frequency (MHz), and thickness of the EMI shield (cm), respectively. The first two terms of the equation represent shielding due to reflection, while the third term accounts for shielding from absorption; multireflection is neglected in this equation. From Simon's formula, the overall shielding performance of a CNT film can be enhanced by either increasing the electrical conductivity or thickness. As shown in Fig. 4c, the calculated $SE_T$ values from Simon's formula follow the same trend as the measured

$SE_T$ values, which increase with an increase in thicknesses.

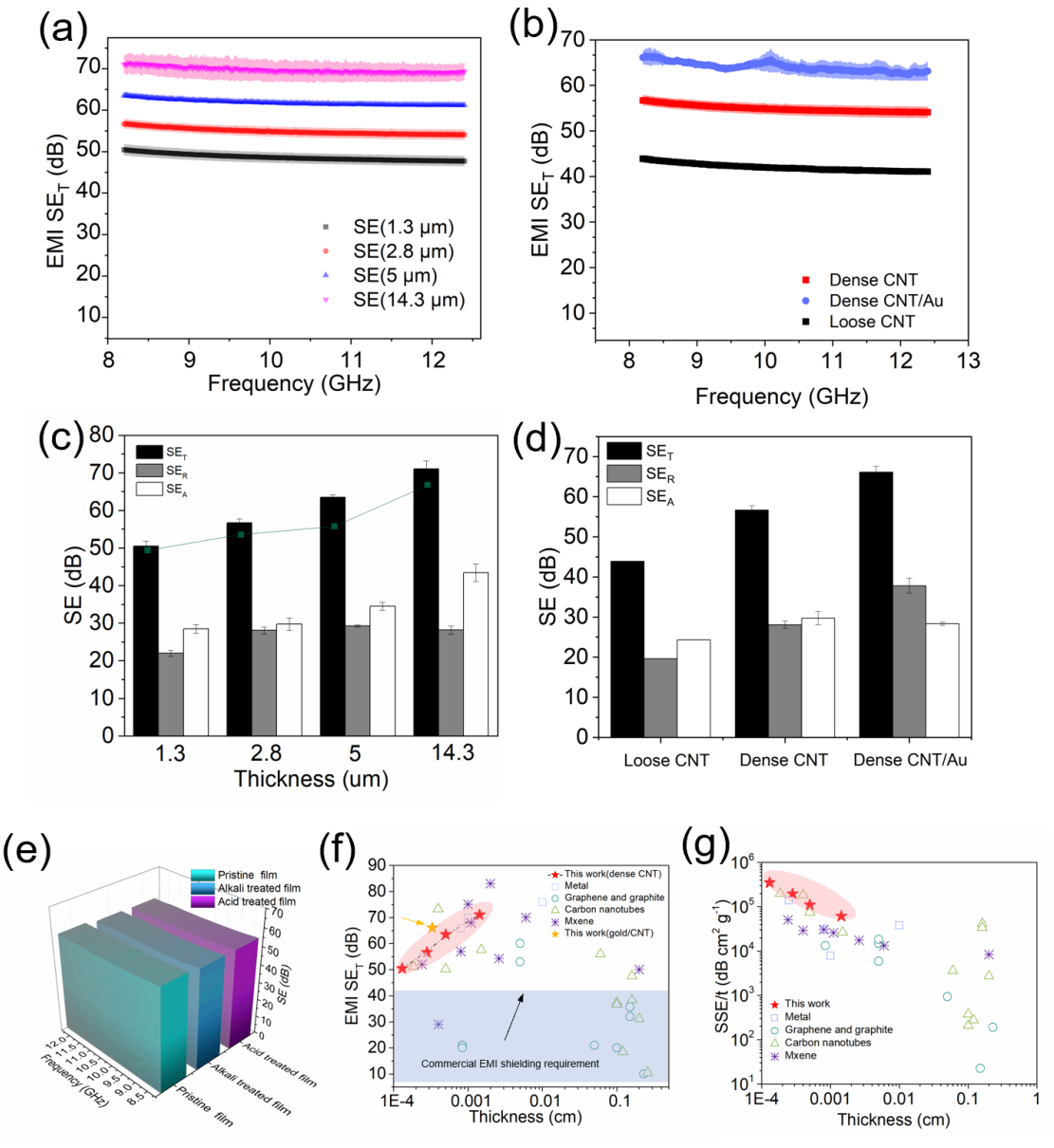


**Fig. 4**. (a) Variances of total $SE_T$ over X band for dense CNT films with different thicknesses (1.3 $\mu$m, 2.8 $\mu$m, 5 $\mu$m, and 14.3 $\mu$m). (b) $SE_T$ over X band for loose CNT film, dense CNT film, and dense CNT/Au film. (c)Measured $SE_T$, calculated $SE_T$ from Simon's formula, and measured absorption ($SE_A$) and reflection ($SE_R$) in dense CNT films at 8.2 GHz. (d) Measured $SE_T$, $SE_A$, and $SE_R$ for loose CNT film, dense CNT film, and dense CNT/Au film. (e) $SE_T$ of pristine dense CNT

353 film, acid treated CNT film, and alkali treated CNT film over X band. (f) Comparison of EMI $SE_T$
354 with the previously published data of metals, graphene and graphite, Carbon nanotube, and
355 MXenes. (g) Comparison of absolute SE with the previously published data of metals, graphene
356 and graphite, Carbon nanotube, and MXenes.

357 To identify the mechanism responsible for the observed EMI shielding in the dense CNT film,
358 the contributions from absorption ($SE_A$), reflection ($SE_R$), and multi-reflection ($SE_M$, which is
359 generally negligible when the $SE_T$ is larger than 15 dB) [3] are determined and compared (Fig. 4c).
360 As mentioned earlier, it has been observed that the $SE_T$ tends to increase with an increase in
361 thickness. In the case of the films under investigation $SE_A$ values consistently surpass $SE_R$ values
362 across all thicknesses. This finding suggests that absorption plays a more prominent role in
363 determining the EMI shielding capability of dense CNT films within the range of 1.3 – 14.3 μm.
364 Interestingly, $SE_R$ increases from 22 dB (at 1.3 $\mu$m) to 28 dB (at 2.8 $\mu$m), but does not continue to
365 increase beyond this thickness. In contrast, $SE_A$ continuously increases with thickness. This can be
366 attributed to the differences between the reflection and absorption processes. Specifically, the
367 incident EM waves first hit the conductive surface of the shielding material where over 99% (20
368 dB) of the EM waves are instantly reflected due to the impedance mismatch[11, 46]. The residual
369 energy (<1%) of the EM waves can penetrate the material, but is attenuated throughout the depth
370 of the film. These penetrated waves are either directly absorbed by ohmic losses[5], due to the
371 occurrence of EM field-induced current that produces thermal energy[47] [48], or reflected at first
372 and then absorbed by adjacent CNTs. In other words, the reflection of EM waves is mainly
373 impacted by a film's electrical conductivity, while EM wave absorption happens throughout the
374 material leading to an increase in absorption with an increase of thickness. A material's electrical
375 conductivity has a large impact on $SE_R$ and $SE_A$ values, albeit to a different degree, as implied

from Simon's formulism, Eq. (1), which partially explains why $SE_A$ grows more than $SE_R$. $SE_R$ is proportional to the logarithm of the material's electrical conductivity, while $SE_A$ is proportional to the square root of the conductivity. Therefore, changes in conductivity have bigger impacts on $SE_A$ than on $SE_R$. In addition to the excellent conductivity, polar functional groups, such as C-O and C=O, the presence of which was verified using XPS analysis (Fig. 3d), can also contribute to the high $SE_R$ through polarization losses[17]. In Figure 4d, we conducted a comparison of the SE in terms of $SE_T$, $SE_R$, $SE_A$ among the loose CNT film, dense CNT film, and dense CNT/Au film. The loose CNT film exhibited inferior performance in both $SE_A$ and $SE_R$ compared to the dense CNT film and dense CNT/Au film. This can be attributed to its relatively lower conductivity, resulting in a smaller $SE_T$ value. On the other hand, the dense CNT/Au film demonstrated the highest $SE_T$ and $SE_R$ among the three films, while $SE_A$ was comparable to that of the dense CNT film. Specifically, the $SE_T$ and $SE_R$ increased by 9.5 dB and 9.7 dB, respectively, while $SE_A$ stabilized at around 29 dB. This suggests that the increase in $SE_T$ was primarily driven by the increase in reflection provided by the gold coating, as gold is well-known for its excellent reflective properties[49]. In our two-layer nanostructured composite, the thin top layer (the Au(0)) with high conductivity primarily serves as a means to reflect EM waves upon initial contact. This layer efficiently redirects the waves away from the material. On the other hand, the thicker secondary nanostructured layer (the CNTs) is designed to absorb and disperse the residual waves that penetrate the top layer. The secondary layer acts as a prolonged pathway for the waves, allowing for multiple reflections and ensuring further attenuation of the EMI. By combining the reflective properties of the thin top layer with the absorbing and multi-reflective capabilities of the thicker secondary layer, the composite provides an effective solution for EMI shielding[50]. As a result,

398 the majority of EM waves (37.8 dB) were reflected by highly conductive dense CNT/gold top
399 surface, the remaining attenuated wave was absorbed and dissipated within the CNT layer.
400 The dense CNT film exhibited robust stability under harsh conditions. The $SE_T$ of dense CNT
401 film remained constant after a 1-hour immersion in acid (1 M $H_2SO_4$ solution) or base (1 M NaOH
402 solution) over the X-band frequency range (Fig. 4e). The high stability of these dense CNT films
403 makes them superior to traditional metallic or polymeric shielding materials that are vulnerable to
404 harsh conditions[51].
405 The EMI $SE_T$ values of our dense CNT film and dense CNT/gold film were compared to values
406 reported for other materials (Fig. 4f and Table S3). In general, carbon-based materials, such as
407 CNTs, graphene, and graphite, are generally found in the right lower corner of Fig. 4e, indicating
408 that they can only achieve a sufficient $SE_T$ at fairly large thicknesses (500 $\mu$m to 1000 $\mu$m), due to
409 their low electrical conductivity. Although metal materials show similar EMI shielding properties
410 compared to our dense CNT films, the high density and poor processibility of metals (i.e.,
411 fabricating them into super thin films) limit their application as EM shields for advanced electrical
412 devices. In contrast, the dense 14.3 $\mu$m thick CNT film in this work displays an extraordinary EMI
413 $SE_T$ of 71 dB, and is not inferior to MXenes with a similar thickness in terms of EMI shielding[4]
414 . The gold/CNT film shows an excellent EMI $SE_T$ of 66.12 dB with 3.3 $\mu$m thickness, which
415 outperforms almost all of the materials we have been studied at such a low thickness.
416 The absolute shielding effectiveness (SSE/t, dB $cm^2$ $g^{-1}$) of the dense CNT films is compared to
417 that of other materials, with the SSE/t value being calculated by dividing $SE_T$ by the product of the
418 material density and thickness (Fig. 4g) [45]. A higher SSE/t value suggests that a given material
419 could achieve a specific SE with a lighter weight and a lower thickness. The dense CNT film shows
420 an impressive SSE/t value that outperforms those exhibited by highly electrically conducting

metals and MXenes. The highest value of SSE/t of 3.6 × $10^5$ dB $cm^2$ $g^{-1}$ was achieved at a thickness of 1.3 $\mu$m, where the SE is 50.5 dB, which is higher than that required for commercial devices (40 dB) [1]. The ability to achieve high SE at low thicknesses and light weight makes dense CNT films an excellent candidate as an EMI shielding material for modern advanced electronics and telecommunication devices.

## 4. CONCLUSIONS

In conclusion, we have reported a CNT film fabrication method that produces metal-like CNT films with robust mechanical strength (161.5 MPa), chemical stability, and high electrical conductivity (779,500 S $m^{-1}$) for carbon-based materials. In addition to its impressive electrical conductivity, the rich functional groups on the dense CNT film contribute to high EMI SE with a very low thickness (i.e., 71 dB at 14.3 $\mu$m). With the addition of the gold coating, the dense CNT/gold membrane exhibits an extremely high conductivity ($2.31\times10^6$ S $m^{-1}$) and EMI SE of 66.12 dB at a total thickness of 3.3 $\mu$m. Furthermore, the dense CNT films are highly stable under harsh conditions and maintain excellent shielding performance after acid/alkali treatment, suggesting their promising potential use in advanced electrical and telecommunication devices.

**Supporting Information**.

The following files are available free of charge.

Electrical conductivity measurement setup, mechanical testing system, XPS spectra, sheet resistance and conductivity of dense CNT films, Mechanical properties, and a comparison table of EMI Shielding effectiveness with that of literature data. (DOC)

Dense CNT film resilience. (MOV)

## Conflicts of interest

The authors declare no competing financial interest.


## ACKNOWLEDGMENT

The authors acknowledge financial support from the National Science Foundation (1926360). In addition, the authors would like to thank the Center for High Frequency Electronics (CHFE) and Minji Zhu for assistance with the vector network analyzer instrument. Additional support for EMVH was provided by the *UCLA Sustainable LA Grand Challenge*. A.A.B acknowledges the support of the Vannevar Bush Faculty Fellowship (VBFF), under contract ONR-N00014-21-1-2947.


## REFERENCES


[1] A. Iqbal, F. Shahzad, K. Hantanasirisakul, M.-K. Kim, J. Kwon, J. Hong, H. Kim, D. Kim, Y. Gogotsi, C.M. Koo, Anomalous absorption of electromagnetic waves by 2D transition metal carbonitride Ti3CNTx (MXene), Science 369(6502) (2020) 446-450.

[2] M. Han, C.E. Shuck, R. Rakhmanov, D. Parchment, B. Anasori, C.M. Koo, G. Friedman, Y. Gogotsi, Beyond Ti3C2Tx: MXenes for Electromagnetic Interference Shielding, ACS Nano 14(4) (2020) 5008-5016.

[3] P. Sambyal, A. Iqbal, J. Hong, H. Kim, M.K. Kim, S.M. Hong, M. Han, Y. Gogotsi, C.M. Koo, Ultralight and Mechanically Robust Ti3C2Tx Hybrid Aerogel Reinforced by Carbon Nanotubes for Electromagnetic Interference Shielding, ACS Appl Mater Interfaces 11(41) (2019) 38046-38054.

[4] F. Shahzad, M. Alhabeb, C.B. Hatter, B. Anasori, S.M. Hong, C.M. Koo, Y. Gogotsi, Electromagnetic interference shielding with 2D transition metal carbides (MXenes), Science 353(6304) (2016) 1137-1140.

[5] Z. Zhou, J. Liu, X. Zhang, D. Tian, Z. Zhan, C. Lu, Ultrathin MXene/Calcium Alginate Aerogel Film for High‐Performance Electromagnetic Interference Shielding, Advanced Materials Interfaces 6(6) (2019).

[6] S.H. Lee, S. Yu, F. Shahzad, W.N. Kim, C. Park, S.M. Hong, C.M. Koo, Density-tunable lightweight polymer composites with dual-functional ability of efficient EMI shielding and heat dissipation, Nanoscale 9(36) (2017) 13432-13440.

[7] S. Lin, H. Wang, F. Wu, Q. Wang, X. Bai, D. Zu, J. Song, D. Wang, Z. Liu, Z. Li, Room-temperature production of silver-nanofiber film for large-area, transparent and flexible surface electromagnetic interference shielding, npj Flexible Electronics 3(1) (2019) 1-8.

[8] G.A. Gelves, M.H. Al-Saleh, U. Sundararaj, Highly electrically conductive and high performance EMI shielding nanowire/polymer nanocomposites by miscible mixing and precipitation, Journal of Materials Chemistry 21(3) (2011) 829-836.
[9] Z. Zeng, F. Jiang, Y. Yue, D. Han, L. Lin, S. Zhao, Y.B. Zhao, Z. Pan, C. Li, G. Nystrom, J. Wang, Flexible and Ultrathin Waterproof Cellular Membranes Based on High-Conjunction Metal-Wrapped Polymer Nanofibers for Electromagnetic Interference Shielding, Adv Mater 32(19) (2020) e1908496.
[10] D.Q. Zhang, T.T. Liu, J.C. Shu, S. Liang, X.X. Wang, J.Y. Cheng, H. Wang, M.S. Cao, Self-Assembly Construction of WS2-rGO Architecture with Green EMI Shielding, ACS Appl Mater Interfaces 11(30) (2019) 26807-26816.
[11] Y. Lin, J. Dong, H. Zong, B. Wen, H. Yang, Synthesis, Characterization, and Electromagnetic Wave Absorption Properties of Composites of Reduced Graphene Oxide with Porous LiFe5O8 Microspheres, ACS Sustainable Chemistry & Engineering 6(8) (2018) 10011-10020.
[12] Y. Li, X. Pei, B. Shen, W. Zhai, L. Zhang, W. Zheng, Polyimide/graphene composite foam sheets with ultrahigh thermostability for electromagnetic interference shielding, RSC Advances 5(31) (2015) 24342-24351.
[13] Z. Barani, F. Kargar, Y. Ghafouri, S. Ghosh, K. Godziszewski, S. Baraghani, Y. Yashchyshyn, G. Cywinski, S. Rumyantsev, T.T. Salguero, A.A. Balandin, Electrically Insulating Flexible Films with Quasi-1D van der Waals Fillers as Efficient Electromagnetic Shields in the GHz and Sub-THz Frequency Bands, Adv Mater 33(11) (2021) e2007286.
[14] I.W. Nam, H.K. Lee, J.H. Jang, Electromagnetic interference shielding/absorbing characteristics of CNT-embedded epoxy composites, Composites Part A: Applied Science and Manufacturing 42(9) (2011) 1110-1118.
[15] M.H. Al-Saleh, U. Sundararaj, Electromagnetic interference shielding mechanisms of CNT/polymer composites, Carbon 47(7) (2009) 1738-1746.
[16] Y. Yang, M.C. Gupta, K.L. Dudley, R.W. Lawrence, Novel carbon nanotube– polystyrene foam composites for electromagnetic interference shielding, Nano letters 5(11) (2005) 2131-2134.
[17] B. Wen, M. Cao, M. Lu, W. Cao, H. Shi, J. Liu, X. Wang, H. Jin, X. Fang, W. Wang, J. Yuan, Reduced graphene oxides: light-weight and high-efficiency electromagnetic interference shielding at elevated temperatures, Adv Mater 26(21) (2014) 3484-9.
[18] B. Shen, W. Zhai, W. Zheng, Ultrathin Flexible Graphene Film: An Excellent Thermal Conducting Material with Efficient EMI Shielding, Advanced Functional Materials 24(28) (2014) 4542-4548.
[19] M.S. Mauter, M. Elimelech, Environmental applications of carbon-based nanomaterials, Environmental science & technology 42(16) (2008) 5843-5859.
[20] T. Ebbesen, H. Lezec, H. Hiura, J. Bennett, H. Ghaemi, T. Thio, Electrical conductivity of individual carbon nanotubes, Nature 382(6586) (1996) 54-56.
[21] W. Xu, Y. Chen, H. Zhan, J.N. Wang, High-Strength Carbon Nanotube Film from Improving Alignment and Densification, Nano Lett 16(2) (2016) 946-52.
[22] M.-F. Yu, O. Lourie, M.J. Dyer, K. Moloni, T.F. Kelly, R.S. Ruoff, Strength and breaking mechanism of multiwalled carbon nanotubes under tensile load, Science 287(5453) (2000) 637-640.

519 [23] W.A. Deheer, W.S. Bacsa, A. Chatelain, T. Gerfin, R. Humphreybaker, L. Forro, D. Ugarte,
520 ALIGNED CARBON NANOTUBE FILMS - PRODUCTION AND OPTICAL AND
521 ELECTRONIC-PROPERTIES, Science 268(5212) (1995) 845-847.
522 [24] E. Bekyarova, M.E. Itkis, N. Cabrera, B. Zhao, A.P. Yu, J.B. Gao, R.C. Haddon, Electronic
523 properties of single-walled carbon nanotube networks, Journal of the American Chemical
524 Society 127(16) (2005) 5990-5995.
525 [25] J. Stallard, W. Tan, F. Smail, T. Gspann, A. Boies, N. Fleck, The mechanical and electrical
526 properties of direct-spun carbon nanotube mats, Extreme Mechanics Letters 21 (2018) 65-75.
527 [26] V.A. Davis, A.N. Parra-Vasquez, M.J. Green, P.K. Rai, N. Behabtu, V. Prieto, R.D. Booker,
528 J. Schmidt, E. Kesselman, W. Zhou, H. Fan, W.W. Adams, R.H. Hauge, J.E. Fischer, Y. Cohen,
529 Y. Talmon, R.E. Smalley, M. Pasquali, True solutions of single-walled carbon nanotubes for
530 assembly into macroscopic materials, Nat Nanotechnol 4(12) (2009) 830-4.
531 [27] O. Kleinerman, L. Liberman, N. Behabtu, M. Pasquali, Y. Cohen, Y. Talmon, Direct
532 Imaging of Carbon Nanotube Liquid-Crystalline Phase Development in True Solutions,
533 Langmuir 33(16) (2017) 4011-4018.
534 [28] Y.J. Wan, X.Y. Wang, X.M. Li, S.Y. Liao, Z.Q. Lin, Y.G. Hu, T. Zhao, X.L. Zeng, C.H. Li,
535 S.H. Yu, P.L. Zhu, R. Sun, C.P. Wong, Ultrathin Densified Carbon Nanotube Film with "Metal-
536 like" Conductivity, Superior Mechanical Strength, and Ultrahigh Electromagnetic Interference
537 Shielding Effectiveness, ACS Nano (2020).
538 [29] H.C. Choi, M. Shim, S. Bangsaruntip, H. Dai, Spontaneous reduction of metal ions on the
539 sidewalls of carbon nanotubes, Journal of the American Chemical Society 124(31) (2002) 9058-
540 9059.
541 [30] D. Wang, P. Song, C. Liu, W. Wu, S. Fan, Highly oriented carbon nanotube papers made of
542 aligned carbon nanotubes, Nanotechnology 19(7) (2008) 075609.
543 [31] P.D. Bradford, X. Wang, H. Zhao, J.-P. Maria, Q. Jia, Y. Zhu, A novel approach to fabricate
544 high volume fraction nanocomposites with long aligned carbon nanotubes, Composites Science
545 and Technology 70(13) (2010) 1980-1985.
546 [32] M. Zhang, S. Fang, A.A. Zakhidov, S.B. Lee, A.E. Aliev, C.D. Williams, K.R. Atkinson,
547 R.H. Baughman, Strong, transparent, multifunctional, carbon nanotube sheets, science 309(5738)
548 (2005) 1215-1219.
549 [33] A.E. Goldt, O.T. Zaremba, M.O. Bulavskiy, F.S. Fedorov, K.V. Larionov, A.P. Tsapenko,
550 Z.I. Popov, P. Sorokin, A.S. Anisimov, H. Inani, J. Kotakoski, K. Mustonen, A.G. Nasibulin,
551 Highly efficient bilateral doping of single-walled carbon nanotubes, Journal of Materials
552 Chemistry C 9(13) (2021) 4514-4521.
553 [34] C. Li, E.T. Thostenson, T.-W. Chou, Dominant role of tunneling resistance in the electrical
554 conductivity of carbon nanotube–based composites, Applied Physics Letters 91(22) (2007).
555 [35] K.Y. Yan, Q.Z. Xue, Q.B. Zheng, L.Z. Hao, The interface effect of the effective electrical
556 conductivity of carbon nanotube composites, Nanotechnology 18(25) (2007).
557 [36] G. Chen, D.N. Futaba, S. Sakurai, M. Yumura, K. Hata, Interplay of wall number and
558 diameter on the electrical conductivity of carbon nanotube thin films, Carbon 67 (2014) 318-325.
559 [37] K.A. Ibrahim, B. Wu, N.P. Brandon, Electrical conductivity and porosity in stainless steel
560 316L scaffolds for electrochemical devices fabricated using selective laser sintering, Materials &
561 Design 106 (2016) 51-59.
562 [38] M.L. Erickson, S.M. Elliott, C.J. Brown, P.E. Stackelberg, K.M. Ransom, J.E. Reddy, C.A.
563 Cravotta, 3rd, Machine-Learning Predictions of High Arsenic and High Manganese at Drinking

Water Depths of the Glacial Aquifer System, Northern Continental United States, Environ Sci Technol (2021).
[39] W. Xin, J.-M. Yang, C. Li, M.S. Goorsky, L. Carlson, I.M. De Rosa, Novel strategy for one-pot synthesis of gold nanoplates on carbon nanotube sheet as an effective flexible SERS substrate, ACS Applied Materials & Interfaces 9(7) (2017) 6246-6254.
[40] B.J. Hinds, N. Chopra, T. Rantell, R. Andrews, V. Gavalas, L.G. Bachas, Aligned Multiwalled Carbon Nanotube Membranes, Science 303(5654) (2004) 62-65.
[41] bruce, Aligned multiwalled carbon nanotube membranes, science.
[42] P. Goh, A. Ismail, B. Ng, Directional alignment of carbon nanotubes in polymer matrices: contemporary approaches and future advances, Composites Part A: Applied Science and Manufacturing 56 (2014) 103-126.
[43] A. Nish, R.J. Nicholas, Temperature induced restoration of fluorescence from oxidised single-walled carbon nanotubes in aqueous sodium dodecylsulfate solution, Physical Chemistry Chemical Physics 8(30) (2006) 3547-3551.
[44] L.-C. Jia, D.-X. Yan, Y. Yang, D. Zhou, C.-H. Cui, E. Bianco, J. Lou, R. Vajtai, B. Li, P.M. Ajayan, Z.-M. Li, High Strain Tolerant EMI Shielding Using Carbon Nanotube Network Stabilized Rubber Composite, Advanced Materials Technologies 2(7) (2017).
[45] T. Yun, H. Kim, A. Iqbal, Y.S. Cho, G.S. Lee, M.K. Kim, S.J. Kim, D. Kim, Y. Gogotsi, S.O. Kim, C.M. Koo, Electromagnetic Shielding of Monolayer MXene Assemblies, Adv Mater 32(9) (2020) e1906769.
[46] H. Xu, X. Yin, M. Zhu, M. Han, Z. Hou, X. Li, L. Zhang, L. Cheng, Carbon Hollow Microspheres with a Designable Mesoporous Shell for High-Performance Electromagnetic Wave Absorption, ACS Appl Mater Interfaces 9(7) (2017) 6332-6341.
[47] Y. Wan, P. Xiong, J. Liu, F. Feng, X. Xun, F.M. Gama, Q. Zhang, F. Yao, Z. Yang, H. Luo, Y. Xu, Ultrathin, Strong, and Highly Flexible Ti3C2Tx MXene/Bacterial Cellulose Composite Films for High-Performance Electromagnetic Interference Shielding, ACS Nano (2021).
[48] Q. Song, F. Ye, X. Yin, W. Li, H. Li, Y. Liu, K. Li, K. Xie, X. Li, Q. Fu, L. Cheng, L. Zhang, B. Wei, Carbon Nanotube-Multilayered Graphene Edge Plane Core-Shell Hybrid Foams for Ultrahigh-Performance Electromagnetic-Interference Shielding, Adv Mater 29(31) (2017).
[49] J. Li, H. Liu, J. Guo, Z. Hu, Z. Wang, B. Wang, L. Liu, Y. Huang, Z. Guo, Flexible, conductive, porous, fibrillar polymer–gold nanocomposites with enhanced electromagnetic interference shielding and mechanical properties, journal of materials chemistry C 5(5) (2017) 1095-1105.
[50] B. Zhou, G. Han, Z. Zhang, Z. Li, Y. Feng, J. Ma, C. Liu, C. Shen, Aramid nanofiber-derived carbon aerogel film with skin-core structure for high electromagnetic interference shielding and solar-thermal conversion, Carbon 184 (2021) 562-570.
[51] Y. Wang, X. Jing, Intrinsically conducting polymers for electromagnetic interference shielding, Polymers for Advanced Technologies 16(4) (2005) 344-351.